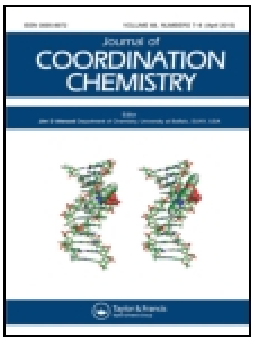

Taylor & Francis
Taylor & Francis Group

Journal of Coordination Chemistry

ISSN: 0095-8972 (Print) 1029-0389 (Online) Journal homepage: http://www.tandfonline.com/loi/gcoo20

Syntheses and X-ray structures of heteroleptic octahedral Mn(II)-xanthato complexes involving N-donor ligands

L. Jeremias, M. Nečas, Z. Moravec, Z. Trávníček & J. Novosad

To cite this article: L. Jeremias, M. Nečas, Z. Moravec, Z. Trávníček & J. Novosad (2015) Syntheses and X-ray structures of heteroleptic octahedral Mn(II)-xanthato complexes involving N-donor ligands, Journal of Coordination Chemistry, 68:23, 4242-4254, DOI: 10.1080/00958972.2015.1102228

To link to this article: http://dx.doi.org/10.1080/00958972.2015.1102228

Journal of Coordination Chemistry, 2015
Vol. 68, No. 23, 4242–4254, http://dx.doi.org/10.1080/00958972.2015.1102228

Syntheses and X-ray structures of heteroleptic octahedral Mn (II)-xanthato complexes involving *N*-donor ligands

L. JEREMIAS*†, M. NEČAS†‡, Z. MORAVEC†, Z. TRÁVNÍČEK§ and J. NOVOSAD†

†Faculty of Science, Department of Chemistry, Masaryk University, Brno, Czech Republic
‡Research Group (Synthesis and Analysis of Nanostructures Structure of Biosystems and Molecular Materials), CEITEC – Central European Institute of Technology, Masaryk University, Brno, Czech Republic
§Faculty of Science, Department of Inorganic Chemistry, Palacký University, Olomouc, Czech Republic

(*Received 3 February 2015; accepted 1 September 2015*)

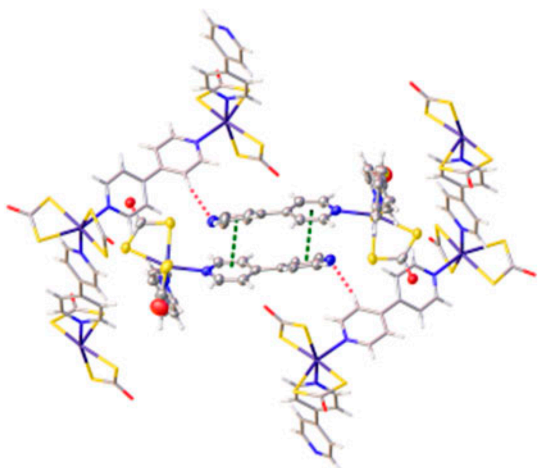

A series of octahedral manganese(II) complexes involving xanthates and *N*-donor ligands, $[Mn(S_2CO\textit{i}Bu)_2(phen)]$ (**1**), $[Mn(S_2CO\textit{i}Bu)_2(2,2'\text{-bpy})]$ (**2**), $[Mn(S_2CO\textit{n}Pr)_2(phen)]$ (**3**), $[Mn(S_2CO\textit{n}Pr)_2(2,2'\text{-bpy})]$ (**4**), $[Mn(S_2COMe)_2(2,2'\text{-bpy})]$ (**5**), $[Mn(S_2CO\textit{n}Pr)_2(4,4'\text{-bpy})]_n$, and $[Mn_2(S_2CO\textit{n}Pr)_4(4,4'\text{-bpy})_3]$ (**6**) (phen = 1,10-phenanthroline, bpy = bipyridine) was prepared. Complexes were characterized by elemental analysis, FTIR spectroscopy, TG/DSC analysis, and single-crystal X-ray diffraction. The structures are built of monomeric molecules of the complexes, except for **6** with the 4,4′-bipyridine ligand, which contains a binuclear complex and 1D polymeric *zigzag* chain in one crystal.

Keywords: Manganese(II) complexes; Crystal structures; Xanthates; Bipyridines; 1,10-Phenanthroline

*Corresponding author. Email: ljeremi@mail.muni.cz

1. Introduction

Xanthates $[ROCS_2]^-$ are 1,1-dithiolates, a group of uninegative, mostly bidentate ligands, that have a wide range of applications in radical polymerization [1, 2], vulcanization of rubber, and biological remediation [3], as collectors in ore beneficiation [4]; metal xanthates can be potentially used as single-source precursors for nanoscopic metal sulfides in photochemical or thermal vapor deposition systems under mild conditions [5].

Coordination compounds involving xanthates in combination with *N*-donor ligands (1,10-phenanthroline, 2,2′-bipyridine, 4,4′-bipyridine or their derivatives) have been studied mostly with zinc and cadmium [6, 7], or nickel [8, 9]. Other metals such as lanthanum [10], europium [11], ruthenium [12], lead [13], and bismuth [14] were also used forming lanthanide(III) complexes with antifungal and antibacterial activities [10], ruthenium dyes with very attractive features for sensitizers in DSSC (dye-sensitized solar cells) [12], and precursors for EuS [11], PbS [13], and Bi_2S_3 [14] nanostructured materials.

Despite the fact that in the Cambridge Crystallographic Data Centre [15] there are hundreds of structures of coordination compounds of xanthate ligands with various metals, only one crystal structure with manganese(II) ([Mn(S_2CO*i*Pr)$_2$(2,2′-bpy)] as two polymorphs [16, 17]) had been reported up to 2010. In that year, two new structures ([Mn(S_2COEt)$_2$(2,2′-bpy)] and [Mn(S_2COEt)$_2$(phen)] [18]) were published, in 2011 the number was increased to four ([Mn(S_2CO*n*Bu)$_2$(py)$_2$], where py = pyridine [19]) and in 2012 the fifth Mn(II)-xanthato complex was characterized by single-crystal X-ray diffraction ([Mn(S_2CO*n*Bu)$_2$(phen)] [20]).

The aim of this work was to synthesize new stable mixed-ligand Mn^{2+} coordination compounds containing methyl, *n*-propyl, or isobutyl xanthate ligands in combination with nitrogen-containing heterocycles (1,10-phenanthroline; 2,2′- or 4,4′-bipyridine), which could stabilize the oxidation state of manganese(II) (complexes with manganese–sulfur bonds can be easily oxidized by atmospheric oxygen [16]), and characterize the prepared complexes by elemental analysis, FTIR spectroscopy, TG/DSC analysis, and single-crystal X-ray diffraction.

2. Experimental

2.1. *Materials and instruments*

Potassium salts of xanthate ligands were prepared according to the literature procedure [21], other reagents and solvents ($Mn(CH_3COO)_2 \cdot 4H_2O$, 1,10-phenanthroline·$H_2O$, 2,2′-bipyridine, 4,4′-bipyridine, chloroform, acetone, *n*-hexane, and acetonitrile) were obtained commercially (Sigma-Aldrich) and used without purification.

Elemental analyses (C, H and N) were performed on a Fisons Instruments EA 1108. Infrared (IR) samples were prepared as KBr pellets and spectra were obtained from 4000 to 400 cm^{-1} using a Bruker IFS 28 spectrometer. Thermal analysis (TG/DSC) was measured on a Netzsch STA 449C Jupiter apparatus from 30 to 200 °C under flowing nitrogen (70 cm^3 min^{-1}) with a heating rate of 10 K min^{-1}.

2.2. *Synthesis of [Mn(S_2COiBu)$_2$(phen)] (1)*

An aqueous solution of K[S_2CO*i*Bu] (0.250 g, 1.32 mmol in 25 cm^3 H_2O) was added dropwise to a stoichiometric amount of $Mn(CH_3COO)_2 \cdot 4H_2O$ (0.163 g, 0.665 mmol) and

1,10-phenanthroline·H_2O (0.132 g, 0.666 mmol) in water (50 cm^3). The mixture was stirred for 30 min and the formed precipitate was filtered off, washed with water, and dried in a desiccator. A yellow-orange powder of **1** was obtained (yield: 0.300 g, 85%; TG: 132.4–141.2 °C Δm = −25.01%; DSC: the maximum of endo-effect at 138.6 °C). Elemental Anal Calcd (%) for **1**, $C_{22}H_{26}MnN_2O_2S_4$: C, 49.52; H, 4.91; N, 5.25. Found (%) : C, 49.63; H, 5.05; N, 5.53. IR data (KBr, cm^{-1}), major bands: 1190s, 1174 m (ν(C–O)$_{as}$), 1148 m, 1128 m (ν(C–O)$_s$), 1055vs (ν(C–S)). The following peaks are due to 1,10-phenanthroline : 1626, 1593, 1576, 1516, 849, and 731.

Single crystals of **1** suitable for X-ray analysis were obtained from slow evaporation of an acetonitrile solution of **1**.

2.3. *Synthesis of [Mn(S$_2$COiBu)$_2$(2,2′-bpy)] (2)*

The orange powder of **2** was prepared using the same procedure as for **1**, with 2,2′-bipyridine (0.104 g, 0.666 mmol) instead of 1,10-phenanthroline·H_2O. Yield: 0.257 g, 76%; TG: 103.6–159.0 °C Δm = −34.25%; DSC: the maximum of endo-effect at 112.4 °C. Elemental Anal. Calcd (%) for **2**, $C_{20}H_{26}MnN_2O_2S_4$: C, 47.14; H, 5.14; N, 5.50. Found (%): C, 46.96; H, 5.32; N, 5.55. IR data (KBr, cm^{-1}), major bands: 1192s, 1177s (ν(C–O)$_{as}$), 1149 m, 1132 m (ν(C–O)$_s$), 1057vs (ν(C–S)). The following peaks are due to 2,2′-bipyridine : 1596, 1573, and 768.

Single crystals of **2** suitable for X-ray analysis were obtained by slow liquid diffusion of hexane into a chloroform solution of **2**.

2.4. *Synthesis of [Mn(S$_2$COnPr)$_2$(phen)] (3)*

This procedure was essentially identical to that described above for **1**. The quantities used were as follows: K[S_2CO*n*Pr] (0.250 g, 1.43 mmol), $Mn(CH_3COO)_2$·4H_2O (0.176 g, 0.718 mmol), and 1,10-phenanthroline·H_2O (0.142 g, 0.716 mmol). An orange powder of **3** was obtained (yield: 0.276 g, 76%; TG: 73.8–123.5 °C Δm = −11.19%; DSC: the maximum of endo-effect at 109.8 °C). Elemental Anal. Calcd (%) for **3**, $C_{20}H_{22}MnN_2O_2S_4$: C, 47.51; H, 4.39; N, 5.54;. Found (%): C, 47.75; H, 4.53; N, 5.81. IR data (KBr, cm^{-1}), major bands: 1190vs (ν(C–O)$_{as}$), 1136s (ν(C–O)$_s$), 1053vs (ν(C–S)). The following peaks are due to 1,10-phenanthroline: 1623, 1593, 1576, 1519, 845, and 728.

Single crystals of **3** suitable for X-ray analysis were obtained by slow liquid diffusion of hexane into chloroform solution of **3**.

2.5. *Synthesis of [Mn(S$_2$COnPr)$_2$(2,2′-bpy)] (4)*

A yellow-orange powder of **4** was prepared using the same procedure as for **3**, with 2,2′-bipyridine (0.112 g, 0.717 mmol) instead of 1,10-phenanthroline·H_2O. Yield: 0.253 g, 73%; TG: 125.6–131.5 °C Δm = -21.09%, 137.2–151.7 °C Δm = −40.64%; DSC: the maxima of endo-effects at 132.2 and 140.7 °C. Elemental Anal. Calcd (%) for **4**, $C_{18}H_{22}MnN_2O_2S_4$: C, 44.90; H, 4.60; N, 5.82. Found (%): C, 44.93; H, 4.76; N, 5.83. IR data (KBr, cm^{-1}), major bands: 1186s (ν(C–O)$_{as}$), 1144 m, 1132 m (ν(C–O)$_s$), 1051s (ν(C–S)). The following peaks are due to 2,2′-bipyridine: 1599, 1562, and 762.

Single crystals of **4** suitable for X-ray analysis were obtained by slow liquid diffusion of hexane into chloroform solution of **4**.

2.6. *Synthesis of [Mn(S_2COMe)$_2$(2,2′-bpy)] (5)*

This procedure was essentially identical to that described above for **1**. The quantities used were as follows: K[S_2COMe] (0.250 g, 1.71 mmol), Mn($CH_3COO)_2\cdot 4H_2O$ (0.209 g, 0.853 mmol), and 2,2′-bipyridine (0.133 g, 0.852 mmol). A yellow-orange powder of **5** was obtained (yield: 0.243 g, 69%; TG: 123.3–134.0 °C Δm = −38.54%; DSC: the maximum of endo-effect at 130.0 °C). Elemental Anal. Calcd (%) for **5**, $C_{14}H_{14}MnN_2O_2S_4$: C, 39.52; H, 3.32; N, 6.58. Found (%): C, 39.80; H, 3.40; N, 6.64. IR data (KBr, cm^{-1}), major bands: 1204s, 1161s (ν(C–O)$_{as}$), 1136s (ν(C–O)$_s$), 1049vs, 1040vs (ν(C–S)). The following peaks are due to 2,2′-bipyridine: 1596, 1567, and 765.

Single crystals of **5** suitable for X-ray analysis were obtained by slow liquid diffusion of hexane into chloroform solution of **5**.

2.7. *Synthesis of [Mn(S_2COnPr)$_2$(4,4′-bpy)]$_n$ (6)*

An acetone aqueous solution of K(S_2CO*n*Pr) (0.125 g, 0.717 mmol in solution of 20 cm^3 acetone and 10 cm^3 H_2O) was added dropwise to a stoichiometric amount of Mn ($CH_3COO)_2\cdot 4H_2O$ (0.088 g, 0.359 mmol) and 4,4′-bipyridine (0.056 g, 0.359 mmol) in acetone (20 cm^3) and water (10 cm^3). The solution was heated under reflux for 30 min, then filtered, and the clear filtrate was evaporated at room temperature to produce crystals of **6**, which were not stable under ambient condition and decomposed. Consequently, no analyses besides X-ray analysis at low temperature (at which the crystals were stabilized) could be made.

The X-ray analysis revealed that **6** crystallizes as a mixture of [Mn(S_2CO*n*Pr)$_2$ (4,4′-bpy)]$_n$ and [Mn_2(S_2CO*n*Pr)$_4$(4,4′-bpy)$_3$].

2.8. *X-ray crystallography*

Diffraction data were collected on a KUMA KM-4 κ-axis CCD diffractometer with Mo-Kα radiation (λ = 0.71073 Å) at 120(2) K. The structures were solved by direct methods and refined on F^2 by full-matrix least-squares techniques using ShelXTL [22]. All hydrogens were placed at calculated positions and refined as riding on their carrier atoms, allowing for free rotation of rigid methyl groups. One of the *n*-propyl groups in **3** and one of the aromatic rings in **6** were found disordered and were refined over two positions with approximately equal occupancies (51 : 49 and 53 : 47 for **3** and **6**, respectively) using similarity (SIMU) and rigid-bond (DELU) restraints on anisotropic displacement parameters. In addition, the terminal carbon of the C20-C21-C22 *n*-propyl moiety in **6** was also disordered over two sites (64 : 36 ratio). To maintain a correct geometry of hydrogen atoms on the C21 atom, a dummy carbon was created and constrained to share the same site (EXYZ) and anisotropic displacement parameters (EADP) with the fully occupied C21. The two pairs of hydrogens with split occupancies were then refined at C21 and the dummy carbon atoms with respect to alternative C22 positions. Crystal data and refinement parameters are presented in table 1.

Analysis of intermolecular non-covalent contacts was made using PLATON [23, 24] and OLEX2 [25]. Details of selected intermolecular non-covalent contacts are presented in table 3. Molecular drawings were obtained using OLEX2 [25] and ORTEP-3 for Windows [26].

Table 1. Crystal data and structure refinements for **1**–**6.**

Compound	**1**	**2**	**3**	**4**	**5**	**6**
Empirical formula	$C_{22}H_{26}MnN_2O_2S_4$	$C_{20}H_{26}MnN_2O_2S_4$	$C_{20}H_{22}MnN_2O_2S_4$	$C_{18}H_{22}MnN_2O_2S_4$	$C_{14}H_{14}MnN_2O_2S_4$	$C_{41}H_{49}Mn_2N_5O_4S_8$
Formula weight	533.63	509.61	505.58	481.56	425.45	1042.21
Temperature (K)	120(2)	120(2)	120(2)	120(2)	120(2)	120(2)
Crystal system	Monoclinic	Orthorhombic	Triclinic	Tetragonal	Monoclinic	Monoclinic
Space group	$C2/c$	$P\,2_1\,2_1\,2_1$	$P\bar{1}$	$I\bar{4}2d$	$P\,2_1/c$	$P\,2_1/n$
Unit cell dimensions (Å, °)						
a	6.579(2)	11.6551(3)	12.546(3)	21.968(3)	6.9016(5)	11.332(6)
b	18.983(7)	11.9734(3)	15.036(3)	21.968(3)	15.4068(9)	15.803(8)
c	20.073(6)	17.2125(4)	15.196(3)	9.3584(19)	16.8217(11)	27.851(12)
α	90	90	101.54(3)	90	90	90
β	99.38(3)	90	112.02(3)	90	94.995(6)	95.40(4)
γ	90	90	112.16(3)	90	90	90
Volume (Å^3)	2473.2(14)	2402.02(10)	2258.3(8)	4516.3(13)	1781.9(2)	4965(4)
Z	4	4	4	8	4	4
Calculated density (Mg m^{-3})	1.433	1.409	1.487	1.416	1.586	1.393
Absorption coefficient (mm^{-1})	0.893	0.916	0.973	0.969	1.217	0.888
HF(000)	1108	1060	1044	1992	868	2156
Goodness-of-fit on F^2	1.000	1.029	1.078	1.147	1.006	1.059
Final R indices [I>2σ(I)]	$R_1 = 0.0245$	$R_1 = 0.0331$	$R_1 = 0.0236$	$R_1 = 0.0210$	$R_1 = 0.0599$	$R_1 = 0.0725$
	$wR_2 = 0.0617$	$wR_2 = 0.0826$	$wR_2 = 0.0656$	$wR_2 = 0.0533$	$wR_2 = 0.1540$	$wR_2 = 0.1696$
R indices (all data)	$R_1 = 0.0339$	$R_1 = 0.0435$	$R_1 = 0.0316$	$R_1 = 0.0223$	$R_1 = 0.1052$	$R_1 = 0.1372$
	$wR_2 = 0.0637$	$wR_2 = 0.0905$	$wR_2 = 0.0704$	$wR_2 = 0.0555$	$wR_2 = 0.1816$	$wR_2 = 0.2030$

3. Results and discussion

3.1. *Synthesis and characterization*

The syntheses of **1**–**6** are described in section 2. Except for **6**, the prepared compounds are stable in air and their experimental values of elemental analyses correspond with the calculated values for coordination compounds with one Mn, two xanthate ligands, and one *N*-donor ligand. According to the TG/DSC analyses, complexes **1**, **4,** and **5** start to decompose at temperatures between 120 and 135 °C, while **2** and **3** start to decompose at lower temperatures (**2** around 100 °C, **3** below 75 °C).

IR spectra of the prepared complexes exhibit bands characteristic for xanthate ligands at 1204–1161 and 1149–1128 cm^{-1} which are associated with asymmetric (C–O) and symmetric (C–O) stretches, respectively. The bands between 1057 and 1040 cm^{-1} may be assigned to ν(C–S) [18]. Compounds **1** and **3** display characteristic peaks from 1,10-phenanthroline at 1626–1516 cm^{-1} and the bands at *ca.* 845 and 730 cm^{-1}. These peaks are shifted with respect to the peaks in the uncoordinated 1,10-phenanthroline (1617, 1587, 1561, 1504, 854, and 739 cm^{-1}) [11]. The characteristic absorptions of 2,2′-bipyridine were at *ca.* 1596, 1565, and 765 cm^{-1} which are in agreement with the bands observed for a similar 2,2′-bipyridine compound [11].

3.2. *Crystal structures*

Crystal structures of the prepared compounds (with the exception of **6** which is discussed separately) are very similar and also to the published structures of [Mn(S_2CO*i*Pr)$_2$(2,2′-bpy)] [16, 17], [Mn(S_2COEt)$_2$(2,2′-bpy)], [Mn(S_2COEt)$_2$(phen)] [18], and ([Mn(S_2CO*n*Bu)$_2$(phen)] [20]. Single-crystal X-ray analysis revealed that the compounds are composed of monomeric molecules (the molecular structures of **1–5** are shown in figure 1). The molecules of **1–5** obey an approximate twofold symmetry, with a twofold axis bisecting the N–Mn–N angle. When viewed along the twofold axis, the MnS_2C rings adhere to the metal in a propeller-like fashion, thus making the molecules chiral. With the exception of **2**, however, the compounds crystallize as racemic mixtures in centrosymmetric space groups.

The manganese ions adopt distorted octahedral coordination geometry formed by four sulfurs of two xanthate ligands and two N of the 2,2′-bipyridine or 1,10-phenanthroline ligands. The Mn–S distances range from 2.5665(17) Å to 2.6686(8) Å. In the reported structures of [Mn(S_2COR)$_2$(L)] (L = 2,2′-bpy, R = Et [18], *i*Pr [16, 17]; L = phen, R = Et [18], *n*Bu [20]) the Mn–S distances range from 2.5651(6) Å to 2.6478(7) Å).

The *S*-ligands and *N*-ligands are all bidentate, forming four- and five-membered MnS_2C, and MnN_2C_2 chelate rings, respectively. Because of restricted ligand bite, the angles N–Mn–N and S–Mn–S are lower than 90° in a regular octahedron. The N–Mn–N angles average at approximately 73.2° and S–Mn–S angles at 69.7° (table 2). These values correspond to the values of published structures (average: 72.7°, and 69.4°, respectively [16–18, 20]). Aromatic rings of 1,10-phenanthroline are generally more coplanar than 2,2′-bipyridine rings as a result of a condensed architecture. The largest RMS deviation from the least-squares plane of the 1,10-phenanthroline rings is observed in **3** (0.0759 Å) in which 1,10-phenanthroline shows a boat-like distortion. A larger flexibility of the 2,2′-bipyridine ligands is apparent from NCCN torsion angles (table 2).

In the case of **1**, the offset head-to-head stacking interactions of the 1,10-phenanthroline rings lead to a staircase-like arrangement, while in the crystal structure of **3**, offset

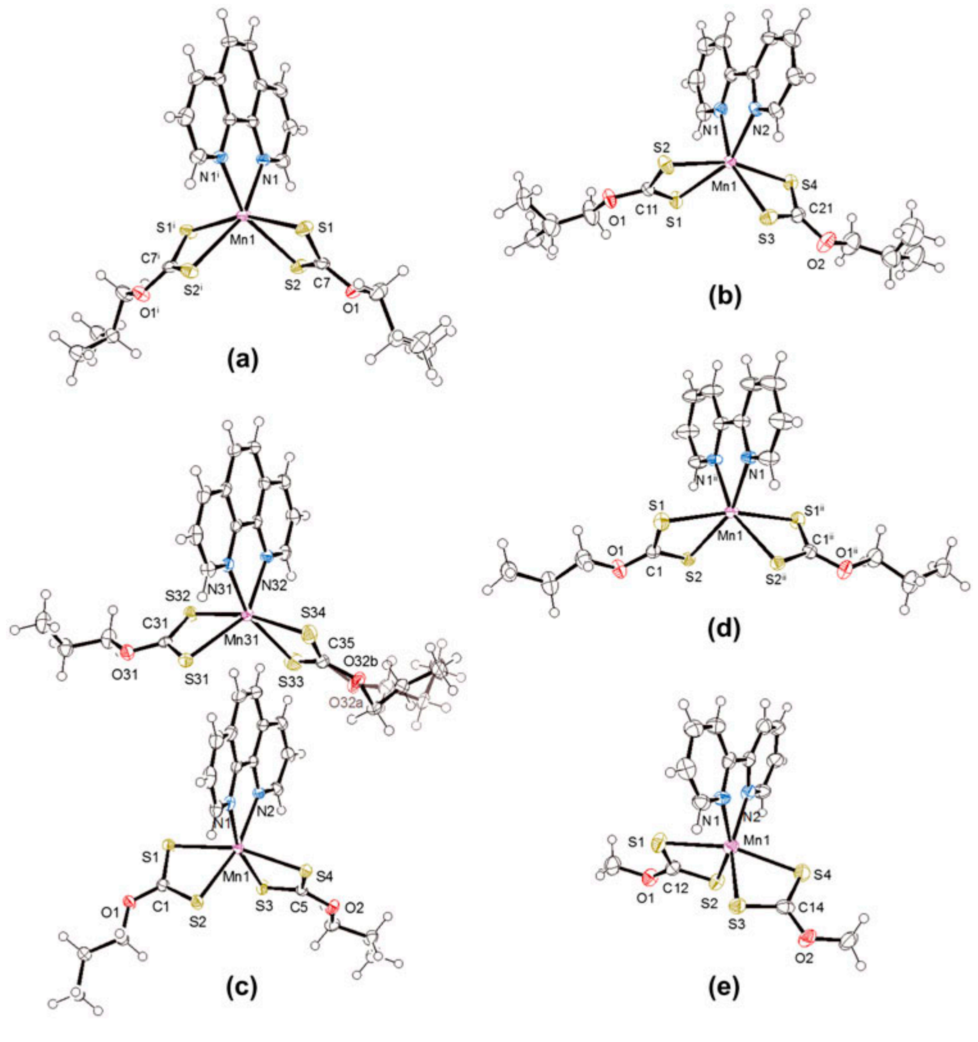

Figure 1. Molecular structures of (**a**) [Mn(S_2CO*i*Bu)$_2$(phen)] (**1**), (**b**) [Mn(S_2CO*i*Bu)$_2$(2,2′-bpy)] (**2**), (**c**) [Mn(S_2CO*n*Pr)$_2$(phen)] (**3**) (there are two crystallographically independent molecules within the asymmetric unit; one of the *n*-propyl groups is disordered)), (**d**) [Mn(S_2CO*n*Pr)$_2$(2,2′-bpy)] (**4**) and (**e**) [Mn(S_2COMe)$_2$(2,2′-bpy)] (**5**) drawn with 50% displacement ellipsoids. Symmetry codes: (i): $1 - x$, y, $1/2 - z$; (ii): x, $1/2 - y$, $5/4 - z$.

head-to-tail stacking interactions of the 1,10-phenanthroline rings can be observed (figure 2, table 3). The parallel displacements of stacked 1,10-phenanthroline ligands in **1** and **3** result in a range of overlaps, including those in which both pyridine and C_6 central rings participate and those in which the ligand edges hardly touch each other when viewed perpendicularly down the stacking direction. The perpendicular distances of 1,10-phenanthroline ligands are comparable to typical interplanar distances found for stacked square-planar complexes with phenanthroline ligands [27].

The distances between the ring centroids in **4** are slightly longer than 4 Å (table 3), giving rise to head-to-tail stacking interactions with a significant overlap of both pyridine rings. Unlike nearly parallel stacking arrangements of the 1,10-phenanthroline ligands in **1** and **3**, the 2,2′-bipyridine ligand stacking planes show a dihedral angle of 19.5° (figure 3).

Table 2. Selected bond lengths (Å) and angles (°) for **1–6** and for published structures.

Coordination compound	Mn–S	Mn–N	N–Mn–N	S–Mn–S	Torsion angle NCCN	Angle between the planes of MnS_2C and MnS'_2C'[a]
$[Mn(S_2CO\mathit{i}Bu)_2$(phen)] (**1**)	2.5825(8) 2.6112(8)	2.2602(15)	73.06(7)	69.43(2)	−3.6(2)	83.37
$[Mn(S_2CO\mathit{i}Bu)_2$(2,2′-bpy)] (**2**)	2.5954(10) 2.5975(10) 2.5761(10) 2.6100(10)	2.266(3) 2.231(3)	72.66(10)	69.86(3) 69.80(3)	−5.8(4)	76.81
$[Mn(S_2CO\mathit{n}Pr)_2$(phen)] (**3**)[b]	2.6085(7) 2.5992(10) 2.618(2) 2.5740(8)	2.261(2) 2.2570(15)	73.34(6)	69.74(2) 70.18(4)	0.7(3)	83.76
	2.6056(9) 2.6686(8) 2.5711(19) 2.5890(8)	2.254(2) 2.2519(15))	73.74(6)	68.67(3) 70.26(4)	−2.6(3)	74.59
$[Mn(S_2CO\mathit{n}Pr)_2$(2,2′-bpy)] (**4**)	2.6047(7) 2.5902(6)	2.2380(17)	73.33(8)	69.740(16)	−2.0(3)	79.52
$[Mn(S_2COMe)_2$(2,2′-bpy)] (**5**)	2.5952(18) 2.6209(17) 2.5673(17) 2.6199(18)	2.260(5) 2.230(5)	73.11(16)	69.31(5) 69.95(5)	15.6(7)	78.30
$[Mn(S_2CO\mathit{n}Pr)_2(4,4'\text{-bpy})]_n$ (**6**) (1D chain)	2.604(2) 2.646(2) 2.637(2) 2.564(2)	2.247(5) 2.257(6)	89.55(19)	68.41(6) 69.50(7)	–	89.97
$[Mn_2(S_2CO\mathit{n}Pr)_4(4,4'\text{-bpy})_3]$ (**6**) (binuclear complex)	2.598(2) 2.670(2) 2.618(2) 2.590(2)	2.261(5) 2.287(5)	88.28(1)	68.22(7) 68.97(6)	–	89.51
$[Mn(S_2COEt)_2$(phen)] [18]	2.5865(7) 2.5895(7) 2.5651(6) 2.6478(7)	2.2470(17) 2.2538(18)	74.17(6)	70.267(17) 69.722(18)	−0.9(3)[a]	74.77
$[Mn(S_2COEt)_2$(2,2′-bpy)] [18]	2.5720(10) 2.6233(10) 2.5881(10) 2.6095(11)	2.270(2) 2.262(2)	72.79(8)	70.18(2) 69.69(3)	−7.8(4)[a]	76.17
$[Mn(S_2CO\mathit{i}Pr)_2$(2,2′-bpy)][c] [16]	2.590(2) 2.616(2)	2.264(2)	71.7(2)	68.99(7)	−15.1 (9)[a]	64.09
$[Mn(S_2CO\mathit{i}Pr)_2$(2,2′-bpy)][d] [17]	2.625(2) 2.556(2) 2.601(3) 2.616(2)	2.247(9) 2.253(8)	71.8(5)	69.17(7) 69.35(8)	−4(2)[a]	71.21
$[Mn(S_2CO\mathit{n}Bu)_2$(phen)] [20]	2.6018(9) 2.5909(9)	2.254(2)	73.22[a]	69.16(3)	−2.8(4)[a]	84.76

[a]Values were generated from program Mercury [31].
[b]There are two crystallographically independent molecules of $Mn(S_2CO\mathit{n}Pr)_2$(phen) in the asymmetric unit.
[c]Orthorhombic unit cell.
[d]Monoclinic unit cell.

Besides the stacking interactions, the C–H···S intermolecular contacts also play a role in the crystal structure arrangement of **1**, **3,** and **5** (figures 2 and 3). The distances of these contacts are slightly shorter than the sum of the contact radii [28], the C···S distances range from 3.399(2) Å to 3.422(3) Å (table S1).

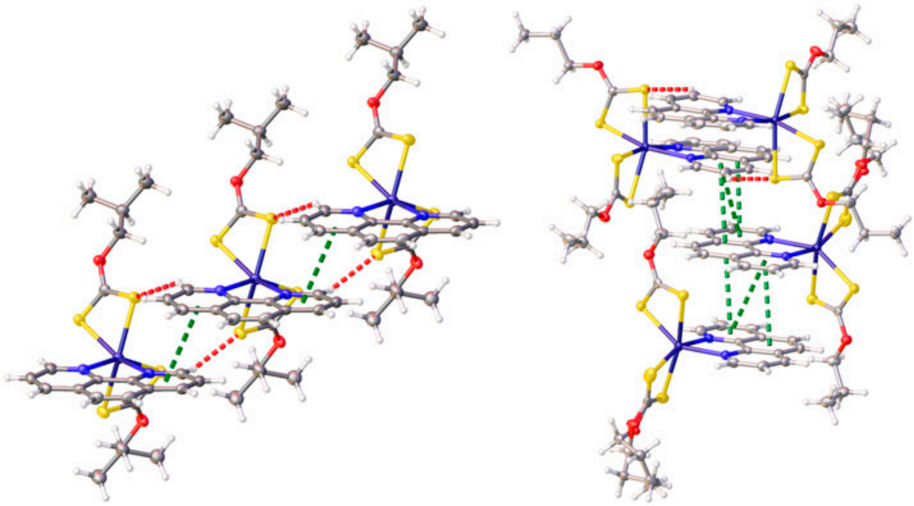

Figure 2. Crystal structures of **1** (left) and **3** (right) showing intermolecular C–H···S non-covalent contacts (red dashed lines) and stacking interactions (green dashed lines).

Table 3. Details of selected stacking interactions (Å) in **1–6**.

Rings and symmetry codes notation:

R1 : N1, C1, C2, C3, C4, and C5 of **1**
R2 : N2, C19, C18, C17, C16, and C20 of **3**
R3 : N32, C49, C48, C47, C46, and C50 of **3**
R4 : C39, C43, C44, C45, C46, and C50 of **3**
R5 : C9, C13, C14, C15, C16, and C20 of **3**
R6 : N31, C39, C43, C42, C41, and C40 of **3**
R7 : N1, C9, C10, C11, C12, and C13 of **4**
R8 : N3, C9, C10, C11, C12, and C13 of **6**
R9 : N4, C14, C15, C16, C17, and C18 of **6**

(*i*): 2-x, y, 1/2-z
(*ii*): -x, 2-y,-1-z
(*iii*): −1-x, 1-y, −2-z
(*iv*): 3/2-x, y, 7/4-z
(*v*): 1-x, -y, -z

I	J	Cg(I)···Cg(J)	Alpha(I, J)	Cg(I)_Perp	Cg(J)_Perp	Δ
[Mn(S₂COiBu)₂(phen)] **(1)**						
R1	R1^{i}	3.7819(18)	4.26(8)	3.4835(7)		1.472
[Mn(S₂COnPr)₂(phen)] **(3)**						
R2	R3^{ii}	3.5788(16)	3.42(11)	3.4248(10)	3.3610(9)	1.038
R2	R4^{ii}	3.9703(16)	2.87(11)	3.4250(10)	3.3876(10)	2.008
R3	R5^{ii}	3.8304(16)	4.71(11)	3.4291(9)	3.2997(10)	1.945
R4	R6^{iii}	3.8560(15)	1.06(11)	3.4121(10)	3.4327(9)	1.757
R6	R6^{iii}	3.6822(16)	0.00(11)	3.4292(9)		1.341
[Mn(S₂COnPr)₂(2,2′-bpy)] **(4)**						
R7	R7^{iv}	4.0167(17)	19.51(12)	3.9092(10)		0.923
[Mn(S₂COnPr)₂(4,4′-bpy)]ₙ and [Mn₂(S₂COnPr)₄(4,4′-bpy)₃] **(6)**						
R8	R9^{v}	3.993(4)	23.2(3)	3.131(2)	3.853(3)	2.478

Notes: Cg···Cg: distance between the ring centroids; Alpha: dihedral angle between the planes; Cg_Perp: perpendicular distance between the centroid Cg and another plane; Δ: shift distance.

Crystals of **6** are composed of two different compounds. The first is a 1D *zigzag* chain coordination polymer with a stoichiometry of $[Mn(S_2CO\textit{n}Pr)_2(4,4'\text{-bpy})]_n$ extending along the crystallographic *b*-direction of the monoclinic cell (figure 4). The *n*-propylxanthates are

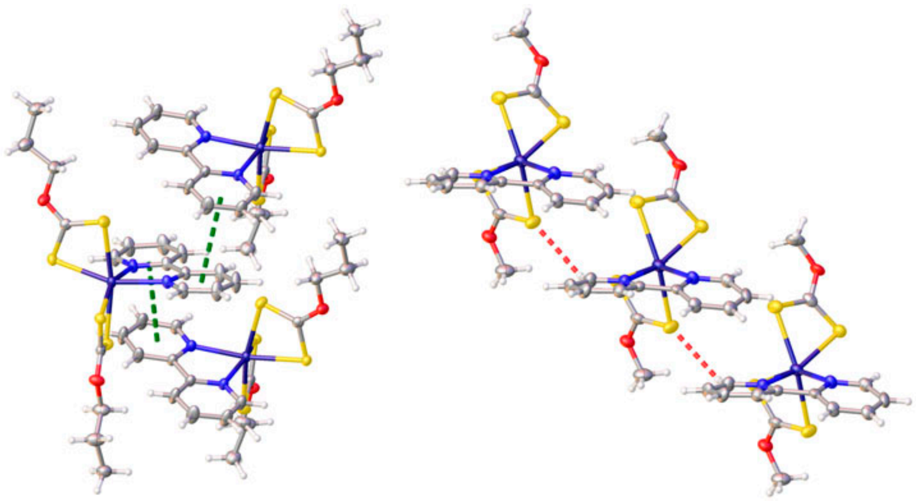

Figure 3. Crystal structures of **4** (left) and **5** (right) showing intermolecular C–H···S non-covalent contacts (red dashed lines) and stacking interactions (green dashed lines).

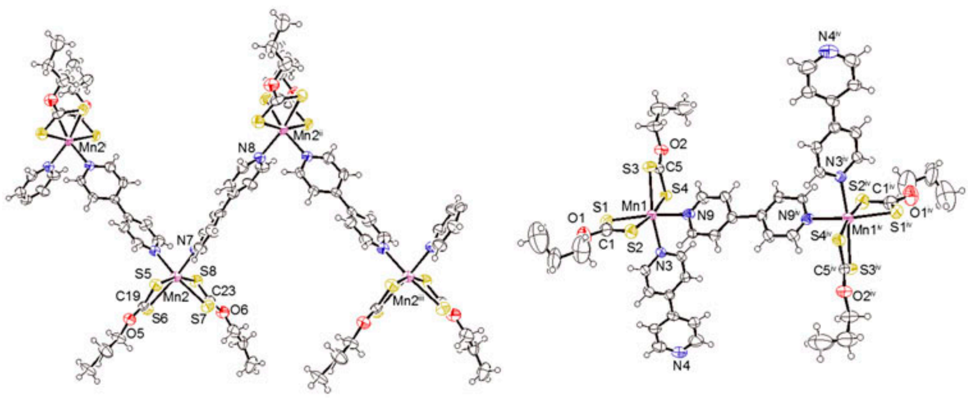

Figure 4. Molecular structure of **6** showing a part of the 1-D polymeric chain $[Mn(S_2CO\textit{n}Pr)_2(4,4'\text{-bpy})]_n$ in a *zigzag* fashion (left) and the binuclear $[Mn_2(S_2CO\textit{n}Pr)_4(4,4'\text{-bpy})_3]$ complex (right) with atoms drawn with 50% displacement ellipsoids. The disordered atoms with minor occupancy have been omitted for clarity. Symmetry codes: (i): $-1/2-x$, $-7/2+y$, $-1/2-z$; (ii): x, $-1+y$, z; (iii): x, $1+y$, z; (iv): $-x$, $1-y$, $-z$.

bidentate ligands forming four-membered MnS_2C chelate rings, while each 4,4′-bipyridine is bridging two Mn ions. The second compound is a binuclear complex $[Mn_2(S_2CO\textit{n}Pr)_4(4,4'\text{-bpy})_3]$ in which two 4,4′-bipyridines are monodentate and the third is bridging. In the crystal, there are thus two independent Mn ions in distorted *cis*-octahedral environments formed by four S of two *n*-propylxanthates and by two N of two different 4,4′-bipyridine ligands. The N–Mn–N angles are close to 90°, while the S–Mn–S angles are considerably lower (68–69°). Unlike the MnS_2C rings in **1–5**, the two MnS_2C planes in **6** are almost perpendicular to each other (table 2).

Complexes containing 4,4′-bipyridine ligands adopt different supramolecular architectures or polymorphs under changing reaction conditions. The reaction of $Zn(SPh)_2$ with 4,4′-bipyridine

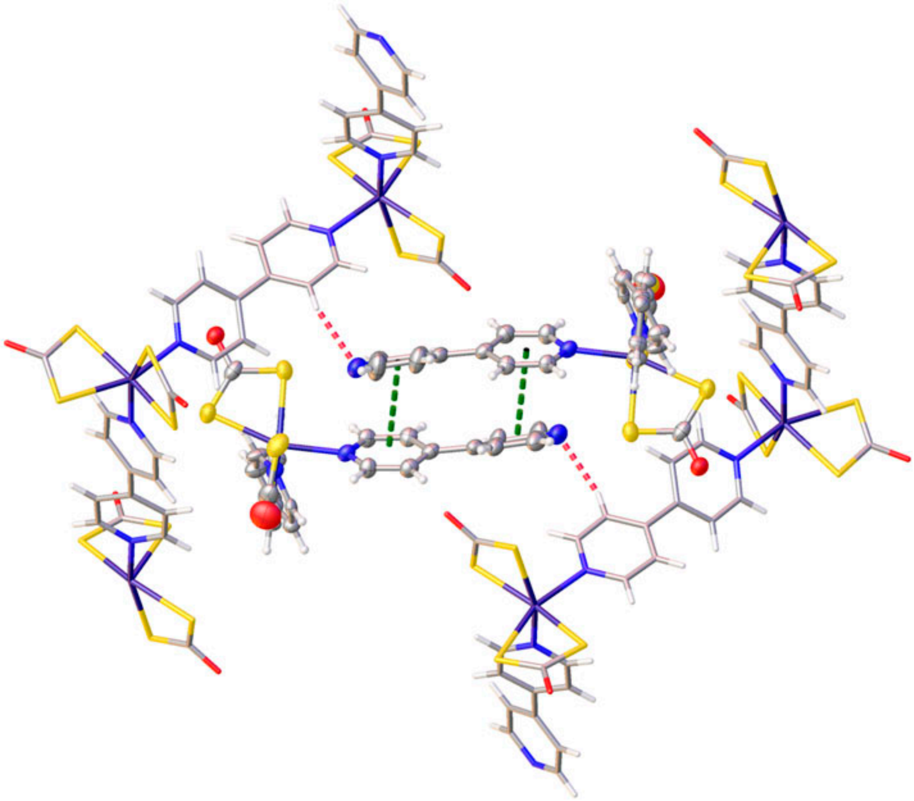

Figure 5. A part of the crystal structure of **6** showing intermolecular C–H···N non-covalent contacts (red dashed lines) and intermolecular stacking interactions (green dashed lines). Polymeric moieties are drawn as "tubes". Symmetrically dependent parts of binuclear complexes and the alkyl chains on O atoms have been omitted for clarity.

yielded either polymeric or binuclear complexes depending on the nature of solvents, reaction time, and method of preparation (diffusion or evaporation techniques) [29]. The effect of pH was previously documented in the reaction system of a Cu(II) salt, 4,4′-bipyridine and benzoic acid [30]. By changing the pH (5.5, 6.0, 7.5, and 8.0), the reaction system provided mononuclear, binuclear, 1D chain, and 2D layer complexes, respectively. However, the crystal structure of **6** seems to be the first in which a polymer and a binuclear complex containing 4,4′-bipyridine crystallize together in one crystal.

The 1D chain and the binuclear complex are linked via the C–H···N intermolecular contacts (table S1), in which the N belongs to the binuclear complex and H to the 4,4′-bipyridine of a 1D chain (figure 5). Stacking dimers based on partially overlapped pyridine rings were observed between the monodentate 4,4′-bipyridine ligands of the binuclear complexes (table 3).

4. Conclusion

We have prepared six new manganese(II) complexes involving xanthates and *N*-donor ligands. Complexes were characterized by elemental analysis, FTIR spectroscopy, TG/DSC analysis, and single-crystal X-ray diffraction. Compound **6** contains a 1D, linear chain coordination polymer extending along the crystallographic *b*-direction of the monoclinic cell, while the other complexes are composed of monomeric molecules and are similar to the published structures with other alkyl chains on the xanthate ligand. Coordination geometries, bond lengths and bond angles in the complexes correspond to the literature data. The crystal packing of complexes is formed via stacking interactions (**1**, **3,** and **6**) and C-H···S (**1**, **3,** and **5**) and C–H···N (**6**) non-covalent contacts. In the extended structure, the molecules are linked by stacking interactions, which occur between the 1,10-phenanthroline or 4,4′-bipyridine ligands. The linkage by C-H···X (X = S or N) non-covalent contacts occurs between the aromatic hydrogens of 1,10-phenanthroline, 2,2′-bipyridine or 4,4′-bipyridine and sulfur of xanthate ligands or nitrogens of 4,4′-bipyridine.

Supplementary material

Details of selected intermolecular non-covalent contacts and alternative positions for disordered parts of compound **6** can be found in the Supplementary Material. X-ray crystallographic files in CIF format have been deposited with the Cambridge Crystallographic Data Centre, CCDC Nos. 928098–928103. These data can be obtained free of charge from The Cambridge Crystallographic Data Centre via www.ccdc.cam.ac.uk/data_request/cif.

Acknowledgements

We would also like to thank to Prof Steinar Husebye (Department of Chemistry, University of Bergen, Norway) for valuable discussion.

Disclosure statement

No potential conflict of interest was reported by the authors.

Funding

This work was supported by the project “Employment of Best Young Scientists for International Cooperation Empowerment” [CZ.1.07/2.3.00/30.0037] co-financed from the European Social Fund and the state budget of the Czech Republic.

Supplemental data

Supplemental data for this article can be accessed http://dx.doi.org/10.1080/00958972.2015.1102228.

References

[1] M.L. Coote, L. Radom. *Macromolecules*, **37**, 590 (2004).
[2] D. Wan, K. Satoh, M. Kamigaito, Y. Okamoto. *Macromolecules*, **38**, 10397 (2005).
[3] E.R.T. Tiekink, I. Haiduc. *Prog. Inorg. Chem.*, **54**, 127 (2005).

[4] G. Winter. *Rev. Inorg. Chem.*, **2**, 253 (1980).
[5] I. Haiduc. In *Handbook of Chalcogen Chemistry New Perspectives in Sulfur, Selenium, and Tellurium*, F.A. Devillanova (Ed.), pp. 593–643, The Royal Society of Chemistry, Cambridge (2007).
[6] L. Jeremias, G. Demo, V. Kubát, Z. Trávníček, J. Novosad, *Phosphorus, Sulfur, and Silicon and the Related Elements*, **189**, 1475 (2014).
[7] M.V. Câmpian, I. Haiduc, E.R.T. Tiekink *Z. Kristallogr. – Cryst. Mater.*, **228**, 187 (2013).
[8] K. Singh, S. Kapoor, R. Sachar, V.K. Gupta, Rajnikant. *X-Ray Struct. Anal. Online*, **28**, 43 (2012).
[9] Z. Trávníček, J. Walla, L Kvítek, Z. Šindelář, M. Biler. *Transition Met. Chem. (Dordrecht, Neth.)*, **24**, 633 (1999).
[10] S. Andotra, N. Kalgotra, S.K. Pandey. *Bioinorg. Chem. Appl.*, **2014**, Article ID 780631/1 (2014).
[11] T. Mirkovic, M.A. Hines, P.S. Nair, G.D. Scholes. *Chem. Mater.*, **17**, 3451 (2005).
[12] K.L. McCall, J.R. Jennings, H. Wang, A. Morandeira, L.M. Peter, J.R. Durrant, L.J. Yellowlees, J.D. Woollins, N. Robertson. *J. Photochem. Photobiol., A*, **202**, 196 (2009).
[13] J.M. Clark, G. Kociok-Köhn, N.J. Harnett, M.S. Hill, R. Hill, K.C. Molloy, H. Saponia, D. Stanton, A. Sudlow. *Dalton Trans.*, **40**, 6893 (2011).
[14] Q. Han, J. Chen, X. Yang, L. Lu, X. Wang. *J. Phys. Chem. C*, **111**, 14072 (2007).
[15] F.H. Allen. *Acta Crystallogr., Sect. B: Struct. Sci.*, **58**, 380 (2002).
[16] V.N. Kirichenko, L.A. Glinskaya, R.F. Klevtsova, T.G. Leonova, S.V. Larionov. *J. Struct. Chem.*, **35**, 242 (1994).
[17] R.F. Klevtsova, L.A. Glinskaya. *Zh. Strukt. Khim.*, **38**, 960 (1997).
[18] M.V. Câmpian, I. Haiduc, E.R.T. Tiekink. *J. Chem. Crystallogr.*, **40**, 1029 (2010).
[19] N. Alam, M.A. Ehsan, M. Zeller, M. Mazhar, Z. Arifin. *Acta Crystallogr., Sect. E: Struct. Rep. online*, **67**, m1064 (2011).
[20] G. Kour, A. Kumar, I. Kour, G. Kour, R. Sachar, V.K. Gupta, Rajnikant. *X-ray. Str. Anal. Online*, **28**, 85 (2012).
[21] I. Haiduc. In *Comprehensive Coordination Chemistry II*, J.A. McCleverty, T.J. Meyer (Eds), Vol. 1, pp. 349–376, Elsevier Ltd., Oxford (2004).
[22] G.M. Sheldrick. *Acta Crystallogr. Sect. A*, **64**, 112 (2008).
[23] A.L. Spek. *J. Appl. Cryst.*, **36**, 7 (2003).
[24] A.L. Spek. *Acta Cryst.*, **D65**, 148 (2009).
[25] O.V. Dolomanov, L.J. Bourhis, R.J. Gildea, J.A.K. Howard, H. Puschmann. *J. Appl. Cryst.*, **42**, 339 (2009).
[26] L.J. Farrugia. *J. Appl. Cryst.*, **45**, 849 (2012).
[27] G.V. Janjić, P.V. Petrović, D.B. Ninković, S.D. Zarić. *J. Mol. Model*, **17**, 2083 (2011).
[28] A. Bondi. *J. Phys. Chem.*, **68**, 441 (1964).
[29] J.T. Sampanthar, J.J. Vittal. *J. Chem. Soc., Dalton Trans.*, 1993 (1999).
[30] S.-T. Wu, L.-S. Long, R.-B. Huang, L.-S. Zheng. *Cryst. Growth Des.*, **7**, 1746 (2007).